



Investigation of the Geometrical Parameters Effects on the Performance and the Flow-Field of Cyclone Separators using Mathematical Models and Large Eddy Simulation

Kh. Elsayed* and C. Lacor**

Abstract: The effects of seven geometrical parameters on the cyclone separator performance and the flow field are investigated via eight mathematical models and computational fluid dynamics (CFD) Fluent software. A cyclone separator with tangential inlet was used to estimate the effect of geometrical parameters on the pressure drop and cut-off size (collection efficiency). A prediction model of the pressure drop and cut-off diameter was obtained based on response surface methodology by means of the statistical software. The results show that the vortex finder diameter, the inlet height, the inlet width, and the total cyclone height play an important role in influencing the cyclone performance other than other factors mentioned in publications. The eight mathematical models used in this study, nearly all gave the same conclusion. For more understanding of the effect of the geometrical parameters on the flow field of cyclone separator, Large Eddy Simulation investigations are performed for six test cases.

Keywords: Cyclone Separator, Cyclone Geometry, Response Surface Methodology, Design of Experiment, Mathematical Models, FLUENT, Large Eddy Simulation.

1. Introduction

Cyclones are widely used for removing industrial dust from air or process gases. They are the most frequently encountered type of gas-solid separator in industry. The primary advantages of cyclones are economy, simplicity in construction and ability to operate at high temperature and pressures. The principle of cyclone separation is simple, where the gas-dust mixture enters from the inlet section. Then, the cylindrical body induces a spinning (swirl), vertical flow pattern to the gas-dust mixture. Centrifugal force separates the dust from gas stream, the dust travels to the walls of the cylinder and down the conical section to the dust outlet and the gas exits through the vortex finder from the top. In order to describe the cyclone performance (pressure drop and collection efficiency) there are three approaches, mathematical models, experimental Investigation, and computational fluid dynamics (CFD). The cyclone performance is affected by several parameters, viz.: cyclone geometry (dimensions, shape of inlet section, number of inlets and vortex finder shape), inlet velocity (volume flow rate), dust mass loading, surface roughness. This study is based on a tangential inlet cylinder on cone

* PhD researcher, Department of Mechanical Engineering, Vrije Universiteit Brussel, Pleinlaan 2 -1050 Brussels- Belgium, /Email khairy.elsayed@vub.ac.be.

** Professor, Department of Mechanical Engineering, Vrije Universiteit Brussel, Pleinlaan 2 - 1050 Brussels- Belgium, /Email khairy.elsayed@vub.ac.be.

cyclone, where seven geometrical parameters affect the flow field and performance, viz. the inlet height a , the inlet width b , the vortex finder diameter D_x , the vortex finder length s , the dust outlet diameter B_c , the cylindrical part height h , the total cyclone height H_t as shown in Fig. 1 where D is the cyclone diameter. First the most important geometrical parameters were determined using mathematical modeling and statistical analysis; secondly, the effects of these factors on the flow field were analyzed computationally using large eddy simulation (LES) turbulence model.

2. Mathematical Models

During the past 50 years, interest in particle collection and pressure theories has steadily increased [1]. For estimation of pressure drop the following models were used: Stairmand Model (1949) [2], Barth Model (1956) [3], Core Model presented by Lewellen (1971) [4], Shepherd and Lapple (1940) [5], Casal and Martinez-Bent (1983) [6], Empirical Correlation presented by Ramachandran et al. (1991)[7]. For estimation of cut-off particle diameter the following two models were used: Barth (1956) [3], Iozia and Leith (1989) [8].

2.1. General Barth Model for Pressure Drop and Collection Efficiency

Barth [3] proposed a simple model based on force balance (classified as one of the equilibrium-orbit models). This model enables to obtain the cut size and the pressure drop values [10].

2.1.1 Estimation of pressure drop

Barth subdivided the pressure drop into three contributions: the inlet loss (this loss could be avoided by good design [3]), the loss in the cyclone body, the loss in the vortex finder. The pressure drop in the cyclone body can be estimated from,

$$\Delta P_{body} = \frac{\rho v_x^2}{2} \frac{D_x}{D} \left(\frac{1}{\left(\frac{v_x}{v_{\theta CS}} - \frac{H_t - S}{0.5 D_x} f \right)^2} - \left(\frac{v_{\theta CS}}{v_x} \right)^2 \right) \quad (1)$$

where $v_{\theta CS}$ is the tangential velocity at the control surface CS , Fig. 2

$$v_{\theta CS} = \frac{\pi R_{in} R_x v_x}{ab\alpha + H_{CS}\pi f R_{in}} \quad (2)$$

where f is the friction factor ($f = 0.05$), R_x is the vortex finder radius ($R_x = D_x/2$), v_x is the mean axial velocity in the vortex finder $v_x = Q/(\pi R_x^2)$ where Q is the volume flow rate and H_{CS} is the height of the control surface extending from the bottom of the vortex finder to the cyclone bottom, see Fig. 2. R_{in} is the radial position of the center of the inlet (as shown in Fig. 3), for a slot inlet $R_{in} = R - b/2$, where b is the inlet width and R is the cyclone radius.

In a cyclone with a slot type of rectangular inlet, the inlet jet is compressed against the wall, resulting in a decrease in the area available for the incoming flow and an increase in the

velocity. Barth accounted for this by introducing α , which is defined as the ratio of the moment-of-momentum of the gas in the inlet and the gas flowing along the wall, see Fig. 3. Barth introduced following formula to calculate α ,

$$\alpha = 1 - 0.4 \left(\frac{b}{R} \right)^{0.5} \quad (3)$$

The pressure drop in the vortex finder can be estimated using a semi-empirical approach as,

$$\Delta P_x = \left(0.5 \rho v_x^2 \right) \left(\left(\frac{v_{\theta CS}}{v_x} \right)^2 + K \left(\frac{v_{\theta CS}}{v_x} \right)^{\frac{4}{3}} \right) \quad (4)$$

where K is the vortex finder entrance factor ($K = 4.4$). The total pressure drop $\Delta P = \Delta P_{body} + \Delta P_x$ can be made dimensionless using the average inlet velocity $v_{in} = Q/(ab)$ leading to the so called Euler number based on the area average inlet velocity, $E_{u_{in}}$.

$$E_{u_{in}} = \frac{\Delta P}{0.5 \rho v_{in}^2} \quad (5)$$

2.1.2 Estimation of cut-off size

As mentioned above Barth's model is based on an "equilibrium-orbit model". This model considers the imaginary cylindrical surface CS that is formed by continuing the vortex finder wall to the bottom of the cyclone, Fig. 2. It is based on the force balance of a particle that is rotating in CS at radius R_x . In the outwardly directed centrifugal force is balanced against the inward drag caused by the gas flowing through surface CS and into the inner part of the vortex. Large particles are therefore "centrifuged" out to the cyclone wall, (because centrifugal force is larger than drag force so it will move outside of CS), and small particles are dragged in and escape out via the vortex finder. The particle size for which the two forces balance -the particles that orbit in equilibrium in CS -is taken as the cyclone's x_{50} or cut-off size; it is the particle size that stands a 50–50 chance of being captured. This particle size is of fundamental importance and is a measure of the intrinsic separation capability of the cyclone. Here, all the gas velocity components are assumed constant over CS for the computation of the equilibrium-orbit size. Barth introduced the following formula to calculate the cut-off size, x_{50} [3],

$$x_{50} = \sqrt{\frac{v_{rCS} 9 \mu_g D_x}{\rho_p v_{\theta CS}^2}} \quad (6)$$

3. Design of Experiment (Sensitivity Analysis)

The usual method to optimizing any investigation set-up is to adjust one parameter at a time, keeping all others constant, until the optimum working conditions are found. Adjusting one parameter at a time is necessarily time consuming, and may not reveal all interactions between the parameters. In order to fully describe the response and interactions of any complex system, a multivariate parametric study must be conducted.

3.1 Response Surface Methodology

Response Surface Methodology (RSM) is a powerful statistical analysis technique which is well suited to modeling complex multivariate processes, in applications where a response is influenced by several variables and the objective is to optimize this response. Box and Wilson first introduced the theory of RSM in 1951 [11], and RSM today is the most commonly used method of process optimization. Using RSM one may model and predict the effect of individual experimental parameters on a defined response output, as well as locating any interactions between the experimental parameters which otherwise may have been overlooked. RSM has been employed extensively in the field of engineering and manufacture where many parameters are involved in a process. In order to conduct any RSM analysis one must first design the experiment, identify the experimental parameters to adjust, and define the process response to be optimized. Once the experiment has been conducted and the recorded data tabulated, RSM analysis software models the data and attempts to fit a second order polynomial to this data. It is assumed that the performance of a cyclone is affected by seven geometry factors, viz. a/D , b/D , D_x/D , S/D , h/D , and H/D , while the values of other parameters affecting the cyclone performance are held constant, (gas density and viscosity, particle density, inlet velocity, mass loading, friction factor, cyclone diameter). To study the effect of the seven geometrical parameters on the pressure drop and cut-off size, for three values for each parameter, for full factorial design of experiment $2187(3^7)$ experiments are required. A more suitable design with a limited number of points can be done using Box-Behnken designs which are experimental designs for response surface methodology, devised by Box and Behnken in 1960 [12]. This set-up results in a Box-Behnken design of seven factors demanding only 64 calculations.

The values of Euler numbers and cut-off diameters for the sixty four designs are calculated with the mathematical models discussed before in Sec. II using VISUAL BASIC 6 code wrote by the authors. This is done in three steps, viz: (1) Construct the design using STATGRAPHICS and put these values in a file to read it by the Visual Basic 6 code. (2) Calculate the values of Euler numbers and cut-off sizes using all mentioned models for cyclone performance. (3) Analysis of the results using STATGRAPHICS.

3.2 Analysis of the Result from $E_{u_{Barth}}$

The first step in analysis of response surface design is to determine which factors have a significant impact on the response variables. This is mostly done using a Pareto chart. The standardized Pareto chart for Barth's model for pressure drop (Euler number) is shown in Fig.4 contains a bar for each effect, sorted from most significant to least significant parameter. The length of each bar is proportional to the standardized effect. A vertical line is drawn at the location of the 0.05 critical values for Student's t. Any bars that extend to the right of that line indicate effects that are statistically significant, for more details about statistical analysis refer to some statistical textbook e.g. [13].

From Pareto chart Fig.4, the vortex finder diameter D_x , the inlet height a and the inlet width b appears to be the most significant factors affecting the pressure drop (Euler number). Concerning correlation of variables, the following interactions seem to have important effects: (1) the inlet width b and the vortex finder diameter D_x (i.e. BD). (2) The inlet height a and the vortex finder diameter D_x (i.e. AD). (3) the vortex finder diameter D_x with cyclone height H , (i.e. DF). The most significant effect is that of vortex finder diameter D_x with inverse relation with pressure drop. In general the ratio between the inlet area ($a \times b$) to the exit area

$(\pi D_x^2 / 4)$ has large effect on pressure drop [10]. Fig. 5 shows the main effect of each parameter, reaching to the same conclusion concerning the most significant geometrical parameters. The inlet height a is linearly related to the pressure drop. The effect of changing the inlet width b on the pressure drop is the most important at small values of b as shown in Fig. 5. The effect of H_t is small but its interaction with D_x denoted by DF in the Pareto chart, has a significant effect on the pressure drop. The remaining variables (B_c ; h ; S) have weak effect on the pressure drop as shown from the Pareto chart, Fig. 4 and the main effect plot given in Fig.5.

Figure 5 concluded that changing D_x has a high effect on the pressure drop, with a very rapid decrease in the pressure drop when increasing D_x up to $D_x \approx 0.625$ after which the relation becomes direct. This may be explained as follows: although the pressure loss in the vortex finder decreases with increasing the vortex finder diameter like the case of viscous flow in pipe, the pressure drop in the cyclone body instead will increase due to the decrease of the flow area just after the flow entrance from the inlet region. This analysis indicates the large contribution of the pressure loss in the vortex finder to the total pressure drop (the pressure loss at the entrance, the pressure loss in the cyclone body, and the pressure loss in the vortex finder). From the Box-Whisker plot for D_x , shown in Fig. 6, the relation between the vortex finder diameter and the pressure drop is not linear, and at small values of D_x the pressure drop is large whereas it decreases drastically to nearly one-fifth at $D_x \approx 0.5$. There are strong interaction between b and D_x . (denoted by BD in the Pareto chart Fig.4, a and D_x , (denoted by AD), and between D_x and H_t (denoted by DF). There is a negligible interaction between a and b (denoted by AB), and no interaction between a and H_t (denoted by AF), b and H_t (denoted by BF) as shown in the Pareto chart Fig. 4. The strong interaction between b and D_x is deduced from Fig. 7(b) for a high value of the D_x pressure drop decreases as b increases while for a small value of D_x the relation between pressure drop and b is almost linear with a high gradient, a similar behavior exist between a and D_x (see Fig. 7(a)) but here the relation is linear instead of curvilinear.

This interaction may be explained as that there is an strong interaction between inlet area ($A_i = a \times b$) and exit area ($A_e = \pi D_x^2 / 4$), so:

- If $A_e > A_i$, the pressure drop will decrease if the inlet area increases (either by increasing a or b). This is due to the large contribution to the vortex finder pressure drop which allows some models to estimate the pressure drop in the vortex finder [10].
- If $A_e < A_i$, the pressure drop will increase if the inlet area increases due to large pressure drop in the vortex finder (from the study of viscous flow in pipes there is inverse relation between pressure drop and pipe diameter.)

Figure 8(a) shows the response surface plot of the effect of a and b on the pressure drop. The lowest pressure drop occur at low values of a and b . The response surface of the effect of a and D_x is shown in Fig. 8(b) where the lowest pressure drop occurs at high values of a and D_x . The correlated effect of b and D_x on the pressure drop is highly negative effect as shown in the Pareto chart Fig. 4, Fig. 7(b) and Fig. 8(c) and Fig. 7(b) indicates that at small values of D_x nearly there is no interaction between b and D_x also the interaction effect increases as D_x increases till a point where $D_x \approx 0.625$ at where there nearly no interaction between b and D_x . The effect of H_t also on the pressure drop is very small but it comes into picture due to its strong interaction with D_x as shown in Fig. 4 and Fig. 8 which shows a change in the trend of

the effect of H_t on pressure drop. For high D_x the pressure drop increases with increasing H_t (the pressure drop in this case remains low) while for low D_x there is inverse relation between H_t and pressure drop (the value of pressure drop is also higher), so the best choice is therefore low H_t and high D_x . This is also confirmed in the response surface plot given in Fig. 8(d).

3.3 Analysis of the Result from $x_{50_{Barth}}$

The previous section focused on the optimum design to minimize the pressure drop and this section will focus on the optimum design to minimize the cut-off size.

From the Pareto chart shown in Fig. 9, the most significant effects are the vortex finder diameter D_x , the inlet width b , and the inlet height a . This is similar as when analyzing $E_{u_{Barth}}$, however in this case the cyclone height H_t appears also to be a main factor affecting the cyclone efficiency (cut-off size). The interactions between the variables inlet width b and vortex finder diameter D_x (i.e. BD), and inlet height a and vortex finder diameter D_x (i.e. AD) seem very prominent for the cyclone efficiency. Actually all geometry parameters affect cut-off size but, the most significant effect is that of the vortex finder diameter D_x which has a direct relation with cut-off size. All parameters significantly affecting the pressure drop also affect the cyclone efficiency. Also the cyclone height H_t effect is significant in the study of cut-off size with inverse relation. The effect of most effective parameters is similar as for pressure drop, exceptions are that, the inlet height a gives a direct linear relation with high gradient Fig.10. The effect of changing inlet width b on cutoff size will be significant with nearly linear relation as shown in Fig. 10. The main effect of H_t is significant with inverse relation, while the change of other factors (B_c ; h ; S) have less effect on the cut-off size as shown from the Pareto chart, Fig. 9 and main effect plot, Fig. 10 respectively.

It is clear from Fig. 10 that changing D_x has high effect on pressure drop with very rapid increase in cut-off size with increasing of D_x so the value of cut-off size may be nearly four times its value at small value of D_x . From Box-Whisker plot for D_x , shown in Fig. 11, the relation between vortex finder diameter and cut-off size is not linear, and at small value of D_x cutoff size is small (means high cyclone efficiency) and increases drastically to be nearly four times at $D_x = 0.75$ (comparing the Box-Whisker plot for D_x in $E_{u_{Barth}}$, shown in Fig. 6, the situation is reversed, so increasing D_x will decrease pressure drop and increase cut-off size). There are weak interaction between inlet height and inlet width, and the effect of a on the cut-off size is large for large values of b , with less effect in case of small value of b , as given in Fig. 12, while the effect of a for small D_x is negligible, and only be significant for high values of D_x , as clear from Fig. 12, the same behavior is exist between b with D_x Fig. 12.

Figure 13(a) shows the response surface plot for the effect of a and b on the cut-off size, where the lowest values of cut-off size occurs at low values of a and b (as the case of pressure drop). The response surface for the effect of a and D_x is shown in Fig. 13(b) where the lowest value for cut-off size occurs at low value of D_x whatever of the value of a , and the effect of b and D_x is nearly the same as shown from Fig. 13(c) which was clear from the interaction plot. The effect of H_t and D_x on the cut-off size is given in Fig. 8(d) and the shape of the surface shown is due to direct relation between D_x with cut-off size and inverse relation of H_t with it, from the figure higher values of cut-off size occurs at low values of H_t and high value of D_x , and lower values of cut-off size exist at high values of H_t and low value of D_x .

As a final comment about this analysis, why increasing a , b , D_x increase the cut-off size (decrease the efficiency) is that in case of large a , b , D_x as a ratio of cyclone diameter the swirling motion of particles will be low, so percentage of particles captured (thrown out to the cyclone wall) decreased, for the effect of H_t as we can see from main effect plot in Fig.10, h has small effect on cut-off size while H_t has large effect that means the effect is that of conical section height, that increasing H_t decreases cut-off size which means increase cyclone efficiency, that is because increasing cone height decreases the particle radial velocity and the so the probability of particles to escape with gas decreased.

3.4 Optimization of the Result from $E_{u_{Barth}}$ and $x_{50_{Barth}}$

From the previous analysis the optimal values for the geometrical parameters that minimize the pressure drop are different from the values that minimize the cut-off size; as a result an optimization for the geometrical parameters values is needed. The optimization procedure will maximize a so called desirability function. It is composed of the product of desirability for each response (here the pressure drop and the cut-off size) to a certain power. The general formula for m responses is given by,

$$D = \{d_1^{I_1} d_2^{I_2} \dots d_m^{I_m}\}^{1/(\sum_{j=1}^m I_j)} \quad (7)$$

where d_j is the calculated desirability of the j_{th} response and I_j is an impact coefficient that ranges between 1 and 5 and the default value is 3 (used in this study). By increasing the impact coefficient I_j for response \hat{y}_j more influence is given to their response. The desirability d_j associated with a predicted response \hat{y}_j is defined as,

$$d_j = \begin{cases} 1 & \hat{y}_j < low_j \\ \left(\frac{\hat{y}_j - high_j}{low_j - high_j} \right) & low_j \leq \hat{y}_j \leq high_j \\ 0 & \hat{y}_j > high_j \end{cases} \quad (8)$$

where low_j , $high_j$ are respectively the minimum and maximum value for \hat{y}_j . For more information about statistical models used for multiple response optimization refer to [14] Table 2 depicts the optimum values of the geometrical parameters that minimize the values of pressure drop and cut-off size, the maximal optimum desirability obtained equals 0.998 resulting in $E_{u_{Barth}} = 30.650$ and $x_{50_{Barth}} = 0.276$. The table also gives the geometrical parameter values that result in worst performance. The minimal desirability equals 0.515887 resulting in $E_{u_{Barth}} = 47.0915$ and $x_{50_{Barth}} = 0.704166$.

4. Computational Study Using Large Eddy Simulation (LES)

The conventional method of predicting the flow field and the collection efficiency of cyclone separator is experimental or via mathematical models. Recently application of computational fluid dynamics (CFD) for the numerical calculation of the gas flow field in a cyclone is becoming more popular [15]. One of the first CFD simulations was done by Griffiths and Boysan[16] who found that the CFD simulations is able to predict the salient features of the

fluid dynamics of cyclone separator, and this method of analysis is almost certainly less expensive than experiment, and represents a cost-effective route for design optimization.

To understand the effect of the geometrical parameters on the flow field of cyclone separator six test cases are simulated computationally via FLUENT with large eddy simulation. The details of the values of the geometrical parameters are given in Table 1.

Table 1: Critical Values of Geometrical Parameters

Factor	a/D	b/D	B_c/D	D_x/D	h/D	H_f/D	S/D	E_u	x_{50}
Min. value	0.250	0.150	0.250	0.250	1.000	3.000	0.500	-	-
Center value	0.375	0.263	0.375	0.500	1.500	4.000	0.750	-	-
Max. value	0.500	0.375	0.500	0.750	2.000	5.000	1.000	-	-
Min. ΔP	0.377	0.375	0.375	0.745	1.998	3.990	0.749	0.000	1.336
Max. ΔP	0.499	0.364	0.250	0.250	1.366	3.107	0.971	65.589	0.531
Min. x_{50}	0.500	0.150	0.250	0.252	1.012	4.395	0.811	43.140	0.246
Max. x_{50}	0.500	0.369	0.306	0.741	1.009	3.138	1.000	0.000	1.917
Optimum design	0.304	0.184	0.250	0.259	1.019	4.799	0.814	30.593	0.277
Worst design	0.466	0.375	0.261	0.322	1.251	3.011	1.000	47.124	0.703

5. Results and Discussion from CFD Simulation

5.1 The pressure field

The contour plots for static pressure for the six cyclones presented in table 2 show that: the static pressure decreases radially from wall to center, with a negative pressure zone appearing in the forced vortex region (central region due to high swirling velocity) so some particles can escape if they enter this zone. The pressure gradient is the largest along radial direction as a highly intensified forced vortex exists, while the gradient in axial direction is small. The flow in the cyclone is not axi-symmetric (due to one inlet section). Two vortical motions exist one moving down (outer vortex) and the other moving up (inner vortex). Both are clear in the contour plot of axial and tangential velocities. Also a large region of negative pressure exists at the central region of all cyclones.

The maximum value for static pressure is that for the case of maximum pressure drop, which has the smallest vortex finder diameter. "Vena-Contracta" phenomenon exists at the entrance of the vortex finder which causes excessive pressure drop. Also the inner vortex is very narrow, so the flow in the majority of the cyclone space has a very low velocity and consequently low swirl which affect the collection efficiency. The pressure contours for the case of maximum pressure drop, min. cut-off size and optimum design are rather similar from three aspects: (1) the majority of the flow is at high static pressure. (2) there is a narrow low pressure region. (3) a Vena-Contracta phenomenon exists at the entrance of the vortex finder. The pressure contours for the case of minimum pressure drop, which has the largest vortex finder diameter, show that: (1) the flow field in the cyclone is not symmetric. (2) The low pressure zone is very wide. (3) The inner vortex touches the cone walls which decreases the collection efficiency considerably as some collected particles can reenter the flow field due to high swirl velocity existing in the inner vortex, and then escape from the vortex finder.

For the case of minimum cut-off size the pressure drop is somewhat less than that for maximum pressure drop, but as the cut-off size is inversely proportional to the vortex finder diameter D_x , so here the vortex finder diameter D_x is small also but the inner vortex surface

(CS in Barth's model) is nearly equal the vortex finder diameter D_x , and here again the negative pressure region is very narrow and contained inside the vortex finder. For the case of maximum cut-off size, the pressure drop value is better than that for the cases of maximum pressure drop and minimum cut-off size as is clear from the contour values. Here the pressure contours are nearly similar to the case of minimum pressure drop, but the inner vortex touches the cone surface which is harmful for cyclone performance; also still the pressure drop is larger than that for the case of minimum pressure drop. The flow field of optimum design case is in between that for the cases for minimum pressure drop and minimum cutoff size, with a longer cone to enhance collection efficiency and a moderate value of the vortex finder diameter D_x to optimize the pressure drop and the cut-off size. The inner vortex is nearly cylindrical and does not touch with cone surface. For the worst design case the pressure drop is less than that for the maximum pressure drop but more than its value for all other cases. This case has the shortest cone height. The flow field has a wide region with nearly stagnant flow, also the negative pressure region extend throughout the cyclone from dust outlet till the gas outlet.

The dynamic pressure is the largest at the interface between the forced vortex and the quasi-free vortex zone. The distribution of the dynamic pressure is asymmetrical due to the non symmetry of the tangential velocity (because the cyclone has only one gas inlet, the axis of the vortex does not coincide with the axis of the geometry of the cyclone) as clear from the contour plots for the case of minimum pressure drop. The highest value of dynamic pressure occurs for the case of maximum pressure drop due to the high velocity spot existing in the vortex finder, while the majority of the flow field has small dynamic pressure values. Also the dynamic pressure distribution is more symmetrical than the case for the minimum pressure drop. For the cases of minimum pressure drop and that of maximum cut-off size there is a spot of high dynamic pressure at the lip of the vortex finder due to high velocity; also the asymmetry of the flow field is very clear. The dynamic pressure distribution for the case of minimum cut-off size and that for the optimum performance looks very similar; this can be explained by the nearly equal values vortex finder diameter and cyclone height. The dynamic pressure distribution for the case of maximum cut-off size is different than that for other cases as it has a larger vortex finder diameter and a short cyclone height; also the flow field near the vortex finder lip is completely chaotic due to the large vortex finder diameter. There is a spot all around the lip due to flow acceleration between the cyclone wall and the vortex finder wall. The case of optimum design is in between that for the minimum pressure drop case and that for minimum cut-off size with a longer cyclone to enhance collection efficiency. The case of worst design is in between that for the maximum pressure drop and the maximum cut-off size with nearly the same values for a , b , H , and s . In the flow field for the case of worst design, the region of high static pressure is exactly the same region of low dynamic pressure. i.e. the majority of the flow field has a small velocity (swirl) which leads to low collection efficiency, while the velocity increase considerably via the vortex finder with large energy losses at the entrance of the vortex finder (entrance loss in viscous flow).

5.2 The Tangential Velocity

The tangential velocity distribution is similar to the dynamic pressure distribution meaning that the tangential velocity is the dominant velocity component in the cyclone separator. The value of the tangential velocity equals zero on the wall and the center of the flow field. The high speed gas enters the inlet and is accelerated up to 1.5 ~ 2.0 times the inlet velocity (13.5 m/s).

Then the velocity decreases as the gas spins down along the wall. Before it goes below the vortex finder, the gas flow collides with the follow-up flow and forms a chaotic flow close to the vortex finder outside wall. The gas velocity decreases sharply after that, this is the main cause of the short-circuiting flow and often results in a higher pressure drop (the same phenomenon was detected by other researchers e.g. [17]). Comparing the values of the tangential velocity for all cases, the maximum value occurs in the case of maximum pressure drop, where the maximum tangential velocity is five times the inlet velocity. There is a discrepancy of the tangential velocity patterns exist in the obtained results as follow. For the case of minimum pressure drop, there is a central cylinder with zero tangential velocity, while the majority of the cyclone has nearly the same value as tangential velocity is considerably low this means also low collection efficiency. For the case of maximum pressure drop the tangential velocity values are very high, the flow field can be subdivided into several region according to the values of tangential velocity: (a) very high values at the inlet of the vortex finder. (b) very low values at the cyclone center and around the vortex finder far away from the inlet zone. (c) high values regions in a cylinder with diameter larger than the vortex finder diameter, so the inner vortex touches the cone wall and consequently a decrease in collection efficiency occurs as some particles which were already collected can reenter the ascending flow region. (d) Moderate values in the remaining region of the cyclone. A vena-Contracta phenomenon exists at the entrance of the vortex finder. For minimum cut-off size, the cyclone becomes longer than that of the maximum pressure drop case; in addition the central cylinder of low velocity becomes twisted. Here the maximum velocity decreases to half the value of the maximum pressure drop case. For the case of maximum cut-off size the tangential velocity is small and the flow field is chaotic. The flow with high tangential velocity touches the cone wall leading to a decrease of collection efficiency. For the case of optimum design the flow field pattern is in between that for minimum cut-off size and minimum pressure drop, the geometrical parameter values are also in between. The maximum tangential velocity is larger than that for minimum pressure drop and less than that for minimum cut-off size. The flow field for the worst design case shows a very high velocity (four times the inlet velocity) but here the vortex finder is small and the cyclone is short. The majority of the flow field has high values (three times the inlet velocity).

5.3. The Axial Velocity

The maximum upward axial velocity occurs in the case of maximum pressure drop (eight times the inlet velocity value). In the case of minimum pressure drop the axial velocity values in the entire cyclone are nearly close. The axial velocity distribution for the cases of maximum pressure drop, minimum cut-off size, optimum design and worst design is nearly similar where three categories of values are distinctive: (a) a high axial velocity spot inside the vortex finder. (b) moderate axial velocity values in the vortex finder extend upto the zone underneath. (c) low axial velocity values in the remainder of the cyclone. The axial velocity distribution for the case of maximum cut-off size is similar to that for the case of minimum pressure drop where the majority of the flow field has moderate values while a high axial velocity spot exists at the vortex finder inlet.

5.4. The Radial Velocity

There is a zone right under the vortex finder where gas flows into the vortex finder directly instead of spinning down to the conical section and then flowing upward. In the conical section, the radial velocity is much larger than that of cylinder section. This will drag some particles into the forced vortex and these particles will not be collected. The distribution of the

radial velocity is nearly uniform in the quasi-free vortex area. The distribution of the radial velocity in the forced vortex is eccentric because of the non-symmetrical geometry of the cyclone. The radial velocity is negative (inward flow) in the gas inlet and then becomes zero rapidly. Afterwards it becomes positive due to the effect of centrifugal force around the vortex finder. The values of the radial velocity are very small compared to those of axial and tangential velocity for each case.

6. Conclusion and Future Work

All the geometrical parameters in the cyclone separator affect its performance, so to determine geometrical parameters which are the most significant a statistical analysis based on response surface methodology (RSM) are performed with the aid of robust mathematical models to calculate the values for the pressure drop and cut-off size. The most significant geometrical parameters are the vortex finder diameter (the outlet cross sectional area), the inlet height and width (the inlet cross sectional area) and the cyclone height. In general, small values of the inlet area and high values of cyclone height (cone height) enhance the cyclone performance (low pressure drop and small cut-off size) but increasing D_x will decrease the pressure drop and increase the cut-off size so its value should be optimized to have the best performance as given by table 1. LES investigation was performed on the six extreme cases obtained from the statistical analysis to understand the effect of these geometrical parameters on the flow field pattern. All mathematical models used in this study gave the same conclusion especially about the significance of D_x , a , and b on the cyclone performance.

For future work, the cut-off size and pressure drop from the CFD simulation to be estimated. Also neural network study with the aid of published experimental data to be investigated. Now there are only four significant geometrical parameters is to be studied computationally for optimization of the cyclone geometry to obtain the best performance and more understanding of the effect of geometry parameters on the flow field. Moreover as the most significant parameters are a , b , D_x and H_t so may be separate study for each one will be helpful to get their individual effect on the flow field and performance. Also as the most significant part of the cyclone is the vortex finder so another study to its shape effect on the performance will be valuable.

6. References

- [1] Zhao, B. and Su, Y., 2006. Particle collection theory for cyclone separators: Summary and comparison. *Particle & Particle Systems Characterization* 23, 484–488.
- [2] Stairmand, C. J., 1949. Pressure drop in cyclone separator. *Engineering* 168, 409-412.
- [3] Barth, W., 1956. Design and layout of the cyclone separator on the basis of new investigations. *Brennstoff-Warme-Kraft*, Vol. 8, No. 4, 1956, 1-9.
- [4] Lewellen, W. S., 1971. A review of confined vortex flows. NASA CR-1772.
- [5] Shepherd, C. B. and Lapple, C. E., 1940. Flow pattern and pressure drop in cyclone dust collectors cyclone without inlet vane. *Industrial & Engineering Chemistry*, Vol.32 No. 9, pp 1246-1248.
- [6] Casal, J. and Martnez-Benet, J. M., 1983. A better way to calculate cyclone pressure drop. *Chemical Engineering*, Vol. 90, No.2, pp. 99-100..
- [7] Ramachandran, G., Leith, D., Dirgo, J., Feldman, H., 1991. Cyclone optimization based on a new empirical model for pressure drop. *Aerosol Science and Technology* 15, pp. 135–148.

- [8] Iozia, D. L., Leith, D., 1989. Effect of cyclone dimensions on gas flow pattern and collection efficiency. *Aerosol Science and Technology* 10, 491–500.
- [9] Altmeyer, S., Mathieu, V., Jullemier, S., Contal, P., Midoux, N., Rode, S., Leclerc, J.P., 2004. Comparison of different models of cyclone prediction performance for various operating conditions using a general software. *Chemical Engineering and Processing* 43, 511–522.
- [10] Hoffmann, A. C. and Stein, L. E., 2008. *Gas Cyclones and Swirl Tubes Principle, Design and Operation*, 2nd Edition. Springer.
- [11] Wikipedia, 2008. Response surface methodology. [http://en.wikipedia.org/wiki/Response surface methodology](http://en.wikipedia.org/wiki/Response_surface_methodology).
- [12] Wikipedia, 2008. Box-Behnken designs. [http://en.wikipedia.org/wiki/Box-Behnken design](http://en.wikipedia.org/wiki/Box-Behnken_design).
- [13] Antony, J., 2003. *Design of Experiments for Engineers and Scientists*. Butterworth-Heinemann.
- [14] Polhemus, N. W., 2005. How to perform an optimization experiment using STATGRAPHICS centurion. <http://www.sigmaplus.fr/telecharg/StatG/howto9.pdf>.
- [15] Wang, B., Xu, D., Chu, K., Yu, A., 2006. Numerical study of gas solid flow in a cyclone separator. *Applied Mathematical Modelling* 30, pp. 1326-1342.
- [16] Griffiths, W. D. and Boysan, F., 1996. Computational fluid dynamics (CFD) and empirical modelling of the performance of a number of cyclone samplers. *Journal of Aerosol Science* 27, 281–304.
- [17] Xiang and R. B., Lee, K. W., 2005. Numerical study of flow field in cyclones of different height. *Chemical Engineering and Processing* 44, pp. 877-883.

Table 2: The Time-Averaged Contour Plots for the Six Cyclones

Case	Min. ΔP	Max. ΔP	Min. x_{50}	Max. x_{50}	Optimum design	Worst design
The static pressure [Pa]						
The dynamic pressure [Pa]						
The tangential velocity [m/s]						
The axial velocity [m/s]						
The radial velocity [m/s]						
The velocity magnitude [m/s]						

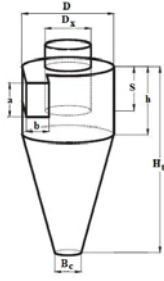


Fig. 1. Schematic diagram for cyclone separator

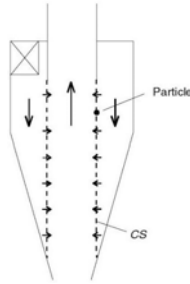


Fig. 2. The control surface concept in Barth model

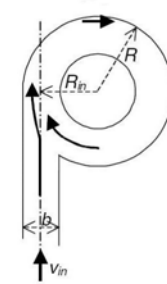


Fig. 3. Inlet flow pattern for slot inlet

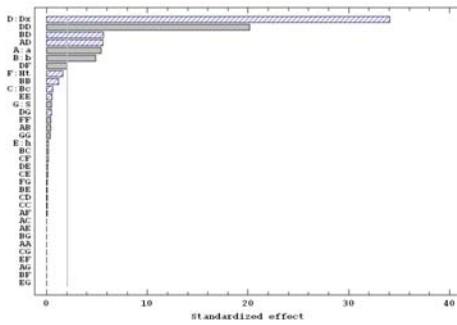


Fig. 4. The Pareto chart for E_{uBarth}

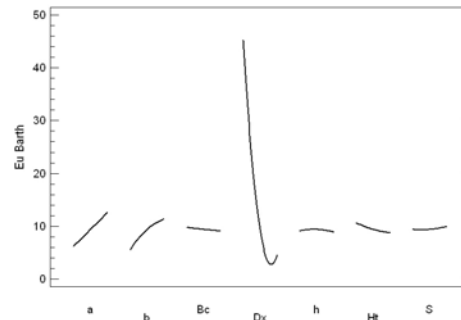


Fig. 5. Main Effects Plot for E_{uBarth}

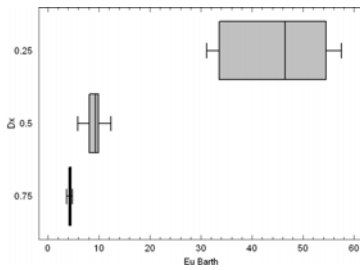
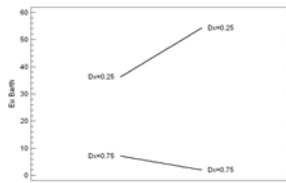
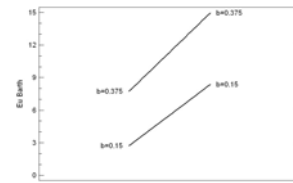


Fig. 6. Box-Whisker Plot for E_{uBarth}

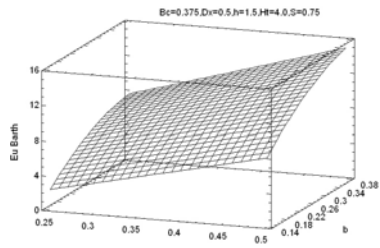


(a) Interaction between inlet height and vortex finder diameter

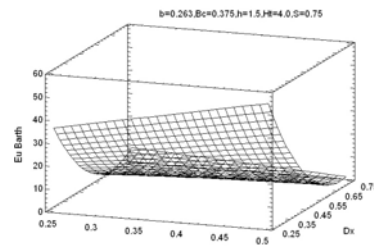


(b) Interaction between inlet width and vortex finder diameter

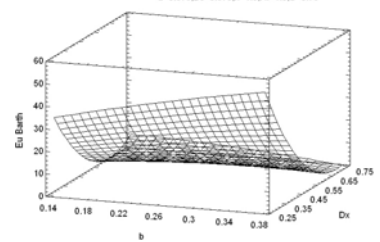
Fig. 7. Interaction Plot for E_{uBarth}



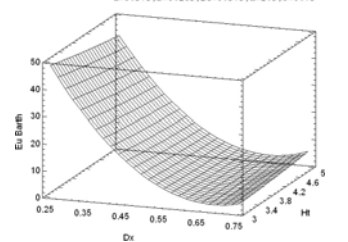
(a) Response surface plot for the effect of a and b



(b) Response surface plot for the effect of a and D_x



(c) Response surface plot for the effect of b and D_x



(d) Response surface plot for the effect of D_x and H_t

Fig. 8. Response Surface Plots for E_{uBarth}

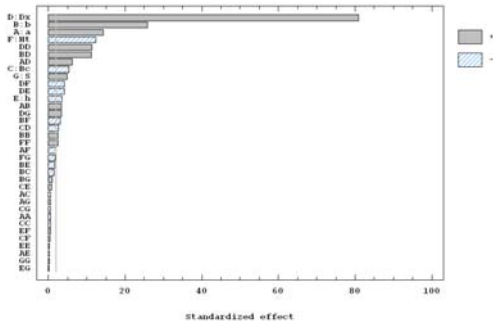


Fig. 9. The Pareto chart for $x50_{Barth}$

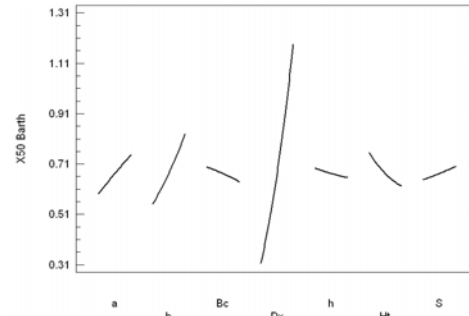


Fig. 10. Main Effects Plot for $x50_{Barth}$

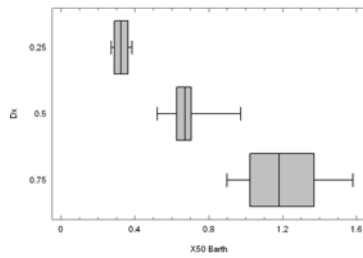
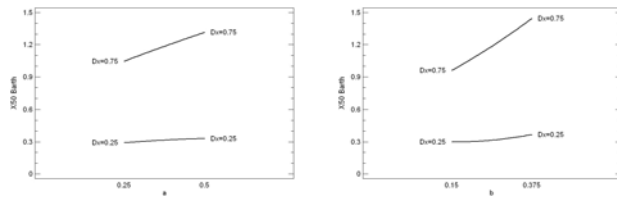


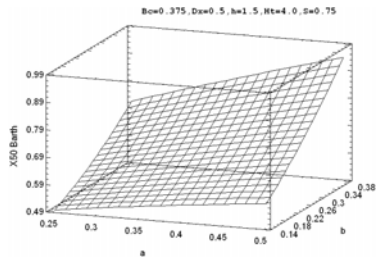
Fig. 11. Box-Whisker Plot for $x50_{Barth}$



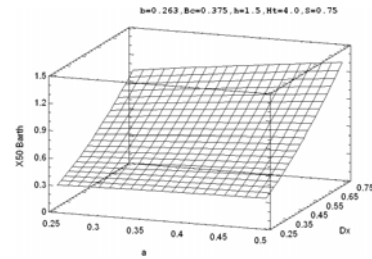
(a) Interaction between inlet height and vortex finder diameter

(b) Interaction between inlet width and vortex finder diameter

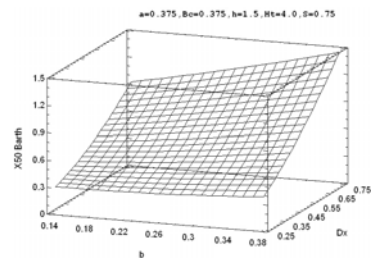
Fig. 12. Interaction Plot for $x50_{Barth}$



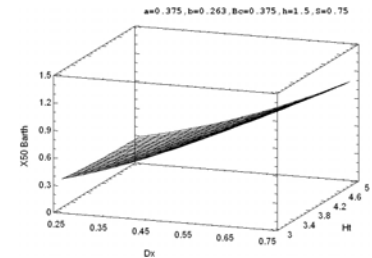
(a) Response surface plot for the effect of a and b



(b) Response surface plot for the effect of a and D_x



(c) Response surface plot for the effect of b and D_x



(d) Response surface plot for the effect of D_x and H_t

Fig. 13. Response Surface Plots for $x50_{Barth}$